



ELSEVIER

Contents lists available at ScienceDirect

Chinese Medical Journal Pulmonary and Critical Care
Medicinejournal homepage: www.elsevier.com/locate/pccm

Original Article

Parkin deficiency aggravates inflammation-induced acute lung injury by promoting necroptosis in alveolar type II cells

Meiyu Quan^{a,1}, Qiang Guo^{b,1}, Xihua Yan^b, Chenhua Yu^c, Linglong Yang^c, Yuting Zhang^d,
Jiaqi Li^c, Qiongxia Weng^b, Bin Liu^a, Quan Li^b, Li Dong^a, Junjie Chen^a, Zhenkun Lou^e,
Xuru Jin^d, Chengshui Chen^{d,*}, Jin-San Zhang^{c,d,e,*}^a Zhejiang Key Laboratory of Interventional Pulmonology; Department of Pulmonary and Critical Care Medicine, The First Affiliated Hospital of Wenzhou Medical University, Wenzhou, Zhejiang 325000, China^b School of Pharmaceutical Sciences, Wenzhou Medical University, Wenzhou, Zhejiang 325035, China^c Medical Research Center; The Zhejiang Key Laboratory of Intelligent Cancer, Biomarker Discovery and Translation, The First Affiliated Hospital of Wenzhou Medical University, Wenzhou, Zhejiang 325000, China^d Department of Pulmonary and Critical Care Medicine, The Quzhou Affiliated Hospital of Wenzhou Medical University, Quzhou People's Hospital, Quzhou, Zhejiang 324000, China^e Department of Oncology, Mayo Clinic, Rochester, MN 55905, USA

ARTICLE INFO

Edited by: Peifang Wei

Keywords:

Acute lung injury
Parkin
Necroptosis
Alveolar type 2 (AT2) cells
Inflammation
Fibrosis
Transgenic mouse models

ABSTRACT

Background: Necroptosis is a form of programmed cell death resulting in tissue inflammation due to the release of intracellular contents. Its role and regulatory mechanism in the context of acute lung injury (ALI) are unclear. Parkin (Prkn), an E3 ubiquitin ligase, has recently been implicated in the regulation of necroptosis. In this study, we aimed to investigate the role and mechanism of Parkin in the process of ALI.

Methods: Lipopolysaccharides (LPS)-induced mouse ALI model was utilized, and the pathological changes in lung tissues were characterized. To elucidate the roles of Parkin and necroptosis in this context, mixed lineage kinase domain-like (Mkl1) knockout mice, Prkn conditional knockout mice, and the necroptosis inhibitor were employed. Additionally, alveolar type 2 (AT2) cell-specific Parkin deletion and lineage-tracing mice were introduced to explore the specific roles and mechanisms of Parkin in AT2 cells.

Results: A dose-dependent increase in Parkin expression in mouse lung tissues following LPS administration was observed, correlating with a shift from epithelial apoptosis to necroptosis. Notably, depletion of MLKL significantly mitigated the pathological changes associated with ALI, particularly the inflammatory response. Conversely, the deletion of Parkin exacerbated the injury pathology, significantly enhancing necroptosis, particularly in AT2 cells. This led to increased inflammation and post-LPS fibrosis. However, treatment with GSK872, a necroptosis inhibitor, substantially mitigated the phenotype induced by Parkin deletion. Importantly, Parkin deletion impaired the proliferation and differentiation of AT2 cells into AT1 cells.

Conclusions: These findings underscore the multifaceted role of Parkin in the progression of lung injury, inflammation, and fibrosis through the regulation of AT2 cell necroptosis. Therefore, Parkin may hold potential as a therapeutic target for managing lung injury and fibrosis.

Introduction

Acute lung injury (ALI) constitutes a critical pulmonary emergency severely jeopardizing human health. Various life-threatening conditions such as severe infections, shock, trauma, and burns can damage alveolar epithelial cells and pulmonary capillary endothelial cells, culminating in

ALI, which generally accompanies intense pulmonary inflammation and increased permeability of alveolar capillaries, leading to diffuse interstitial and alveolar edema. This may result in acute hypoxic respiratory insufficiency or respiratory failure. Globally, an estimated 2.2 million individuals suffer from ALI annually, with a high in-hospital mortality rate of around 40%.¹ Moreover, even after surviving the initial acute

* Corresponding authors at: Department of Pulmonary and Critical Care Medicine, The Quzhou Affiliated Hospital of Wenzhou Medical University (Quzhou People's Hospital), Quzhou, Zhejiang 324000, China.

E-mail addresses: Zhang_jinsan@wmu.edu.cn (J.-S. Zhang), Chenchengshui@wmu.edu.cn (C. Chen)

¹ Mei-Yu Quan and Qiang Guo contributed equally to this work.

<https://doi.org/10.1016/j.pccm.2024.11.004>

Received 23 June 2024; Available online 12 December 2024

2097-1982/© 2024 The Author(s). Published by Elsevier B.V. on behalf of Chinese Medical Association. This is an open access article under the CC BY-NC-ND license (<http://creativecommons.org/licenses/by-nc-nd/4.0/>)

injury phase, ALI frequently develops irreversible pulmonary fibrosis, contributing to poor patient prognosis.² Currently, there are no effective clinical treatments for ALI and its associated pulmonary fibrosis. An in-depth comprehension of lung injury and repair mechanisms in ALI, identifying crucial therapeutic targets, remains an urgent clinical challenge.

A critical mechanism in the pathogenesis of ALI involves the impairment of alveolar epithelial cells. Comprising flat alveolar type 1 (AT1) cells and cuboidal alveolar type 2 (AT2) cells, alveolar epithelium forms a highly compact barrier that limits solute passage while facilitating carbon dioxide and oxygen diffusion.³ AT2 cells secrete surfactants such as surfactant protein C (SPC, encoded by the *Sftpc* gene), which are pivotal in reducing surface tension, preventing alveolar collapse, and promoting efficient gas exchange.⁴ AT2 cells possess considerable plasticity and exhibit facultative stem cell characteristics. Studies on lung injury repair mechanisms suggest that AT2 cells swiftly proliferate and differentiate into AT1 cells following epithelial injury.⁴ The regenerative properties of AT2 cells, resembling stem or progenitor cells, include self-renewal and differentiation, crucial for lung injury repair processes.^{5,6} Loss of AT2 cell function during the progression of lung injury leads to more severe lung damage.⁷

Parkin (*Prkn*) is an E3 ubiquitin ligase responsible for poly-ubiquitination and mono-ubiquitination of its substrate proteins.⁸ Protein ubiquitination is a fundamental post-translational modification that regulates protein half-life, fate and function. *Prkn* is a gene associated with neurodegenerative diseases and is commonly regarded as a neuroprotective protein.⁹ Loss-of-function mutations in *Prkn* are the most prevalent cause of a subtype of Parkinson's disease (PD), the autosomal recessive juvenile parkinsonism (ARJP), an autosomal recessive hereditary disorder.^{10,11} Previous research on Parkin has revealed its significant regulatory role in ALI. For instance, in ALI induced by sepsis, the B-cell lymphoma-2 (*Bcl-2*) protein regulates phosphatase and tensin homologue deleted on chromosome ten (*PTEN*) induced putative kinase 1 (*PINK1*)/Parkin signaling to mediate mitochondrial autophagy,¹² while Parkin itself participates in modulating the inflammatory response mediated by lipopolysaccharide (LPS) during ALI.¹³ Studies indicate that Parkin deficiency in chronic obstructive pulmonary disease (COPD) results in increased inflammatory factors such as interleukin (IL)-6, tumor necrosis factor- α (TNF- α), and promotes enhanced nuclear translocation of nuclear factor- κ B (NF- κ B), leading to a heightened inflammatory response.¹⁴ However, the precise role of Parkin in inflammation and lung injury remains unclear.

We previously reported an important role of Parkin in modulating necroptosis-driven inflammatory responses that contribute to tumorigenesis.¹⁵ Our key mechanistic finding is that Parkin regulates formation of necrosomes via promoting the polyubiquitination of receptor-interacting serine/threonine protein kinase 3 (RIPK3). RIPK1 and RIPK3 are central components in the necroptotic pathway and closely tied to inflammatory reactions.¹⁶ RIPK3 acts as the primary initiator of necroptosis pathways, with its phosphorylation facilitating the formation of necroptotic complexes with RIPK1.¹⁷ Parkin is phosphorylated and activated by the cellular energy sensor adenosine monophosphate (AMP)-activated protein kinase (AMPK), which in turn suppresses necrosome formation through promoting polyubiquitination of RIPK3 via lysin 33-linkage.¹⁵ This regulatory mechanism implicates the crucial role of AMPK–Parkin–RIPK3 axis in modulating necroptosis. Furthermore, mixed lineage kinase domain-like (MLKL) plays a crucial role as an executioner in the necroptosis pathway, and ultimately leads to the disruption of cell membranes.¹⁸ When cells undergo necroptosis, they release damage-associated molecular patterns (DAMPs), which stimulate a strong inflammatory response and aggravate tissue damage.

The current study aims to explore the potential role of Parkin in regulating cell death mechanisms associated with ALI. Specifically, we focus on investigating its impact on necroptosis and the heightened inflammatory response observed in LPS-induced severe ALI. To achieve

this, we employed AT2-lineage tracing and *Prkn*, as well as *Mkl1* knockout mouse models. Our findings highlight the pivotal role played by the Parkin–RIPK3–MLKL axis in influencing both lung injury and inflammation.

Methods

Transgenic mouse and lung injury models

Wild-type (WT) and transgenic mice, including *UBC^{Cre-ERT2}*, *Sftpc^{iCre}*, *tdTomato^{lox/+}*, *Mkl1^{-/-}*, *Prkn^{lox/lox}* strains on a C57BL/6 background, were obtained from GemPharmatech Co. Ltd. (Nanjing, Jiangsu, China) and Shanghai Model Organisms Center, Inc. (SMOC) (Shanghai, China), respectively. The mice were housed indoors under controlled environmental conditions, including a constant temperature of $25 \pm 2^\circ\text{C}$, humidity of $60 \pm 10\%$, and a 12-hour light-dark cycle. All animal experiments strictly adhered to the ethical guidelines outlined in the Guide for the Care and Use of Laboratory Animals, as established by Wenzhou Medical University, Wenzhou, China. The experimental protocol received approval from the Institutional Animal Care and Use Committee of the University (No. WYDW2017-0111). The dosage of the drug administered was determined based on the body weight of mice at 8 to 9 weeks old. Tamoxifen, dissolved in corn oil at a concentration of 100 $\mu\text{g/g}$, was injected intraperitoneally (i.p.) every other day, with a total of five injections followed by a 7-day washout period before performing LPS injury. To administer LPS, it was dissolved in saline and delivered to the mice through intratracheal instillation (i.t.). Before sacrifice, the mice were anesthetized with an intraperitoneal injection (i.p.) of 4% chloral hydrate at a dose of 0.1 mL per 10 g of body weight.

Primary and secondary antibodies

For Western blot (WB) analysis, primary antibodies from Abcam (Cambridge, UK), Cell Signaling Technology (Danvers, Massachusetts, USA), Sigma (Livonia, Michigan, USA), and ABways (Shanghai, China) were used. Specifically, MLKL (ab184718), phospho-MLKL (p-MLKL) (ab196436), TNF- α (ab1793), p-RIPK3 (ab205421), RIPK3 (ab62344) were from Abcam; Parkin (4211), cleaved caspase 3 (9664S), and IL-6 (12912S) were from Cell Signaling Technology; α -smooth muscle actin (α -SMA) (C6198) and glyceraldehyde-3-phosphate dehydrogenase (GAPDH) (AB2000) were from Sigma and ABways, respectively. The pre-conjugated secondary antibodies used were horseradish peroxidase (HRP) goat anti-mouse immunoglobulin G (IgG) (heavy chain + light chain, H+L) (SA00001-1) and HRP goat anti-rabbit IgG (H+L) (SA00001-2) from Proteintech (Chicago, IL, USA).

For immunohistochemistry (IHC), the specific primary antibodies used were CD68 (ab283654), p-MLKL (ab196436), TNF- α (ab1793), CD45 (ab10558), and high mobility group box 1 (HMGB1) (ab190377) from Abcam; Parkin (4211) from Cell Signaling Technology; and collagen 1 (GTX26308) from GeneTex (Irvine CA, USA).

For immunofluorescence (IF), the primary antibodies included Parkin (sc-32282) and RAGE (sc-74473) from Santa Cruz Biotechnology (Santa Cruz, CA, USA); p-MLKL (ab196436) from Abcam; anti-surfactant protein C (AB3786) from EMD Millipore (Billerica, MA, USA); and α -SMA (C6198) from Sigma. The secondary antibodies used were donkey anti-rabbit IgG (H+L) 568 (A10042), goat anti-mouse IgG (H+L) 488 (A32723), donkey anti-rabbit IgG (H+L) 488 (A21206), and donkey anti-mouse IgG (H+L) 568 (A10037), all sourced from Invitrogen (Carlsbad, CA, USA).

Bronchoalveolar lavage fluid analysis and Giemsa-Romanowsky stain

To collect the bronchoalveolar lavage fluid (BALF), the mouse lungs were lavaged three times with 1 ml of phosphate buffered saline (PBS)

containing 1% fetal calf serum (FCS) (PBS-1%). Pooled BALF was centrifuged at 400 × g for 5 min at 4°C. The cell pellets were resuspended in 200 µl of PBS-1%, and 20 µl of cell suspension was dropped onto adhesive slides, allowed to air dry. In the designated areas of the slides, 0.5–1 ml of Giemsa-Romanowsky stain (G1020, Solarbio, Beijing, China) was added and left to stand for 10–15 min. Subsequently, an equal volume of distilled water was added, and the slides were gently agitated to thoroughly mix with the Giemsa-Romanowsky staining solution, followed by a 3–5 min incubation period. The slides were then rinsed with distilled water, air-dried, sealed with neutral resin, and examined under an optical microscope.

Lung histology, immunohistochemistry and Masson staining

Lung tissue specimens were fixed in a 4% paraformaldehyde solution (P0099-500 ml, Beyotime, Suzhou, China) for a duration of 24 h. The entire pulmonary tissue edema and hemorrhagic areas were observed to assess the degree of lung injury. Lung tissues were routinely dehydrated, paraffin-embedded, and sectioned at a thickness of 5 µm, followed by staining with a hematoxylin and eosin (H&E) staining kit (G1120, Solarbio). Under high magnification, the alveolar structure was identified, and the lung injury score was assessed based on the thickening of alveolar walls and the shedding of cells between alveoli. The scoring criteria are as follows: 0 points, no injury; 1 point, less than 25% of the injured area; 2 points, 25% to 49% of the injured area; 3 points, 50% to 75% of the injured area; 4 points, greater than 75% of the injured area. IHC staining was performed on separate paraffin slides. Prior to IHC staining, the slides underwent dewaxing, rehydration, and antigen retrieval in a sodium citrate buffer (pH 6.0). The IHC procedure was executed using an ultra-sensitive Streptavidin-Peroxidase (S-P) kit (KIT-9720, MXB, Xiamen, Fujian, China) in accordance with the manufacturer's instructions, utilizing the previously mentioned antibodies. The stained sections were then subjected to color development using a 3,3'-diaminobenzidine (DAB) color development kit (DA1010, Solarbio) as per the manufacturer's guidelines, followed by sealing with neutral resin for subsequent histological examination. For the assessment of pulmonary fibrosis, Masson's Trichrome Stain Kit (G1340, Solarbio) was employed. The stained sections were finally sealed with neutral resin to preserve the results.

Immunofluorescence staining and terminal deoxynucleotidyl transferase (TdT) dUTP nick-end labeling (TUNEL) assay

Lung tissue samples were promptly cryopreserved in liquid nitrogen and embedded in optimal cutting temperature (OCT) compound. The frozen tissue blocks were then precision-sectioned into 6 µm slices using a cryostat. Subsequently, the slides were allowed to equilibrate at room temperature for one hour. Afterward, a 5% bovine serum albumin (BSA) (A8850, Solarbio) blocking step was conducted at room temperature for 60 min. Following this, the sections were incubated with specific primary antibodies. Following a PBS wash, a secondary antibody was applied for one hour at room temperature. Cell nuclei were stained with 4',6-diamidino-2-phenylindole (DAPI) (0100-20, Southern Biotech, Birmingham, Alabama, USA). For the TUNEL assay, lung sections were prepared as described previously,¹⁹ and cell apoptosis was detected using the One Step TUNEL Apoptosis Assay kit (C1086, Beyotime). TUNEL-positive cells were quantified according to the manufacturer's instructions, with the nuclei concurrently labeled with DAPI for visualization.

Propidium iodide staining and the 5-ethynyl-2'-deoxyuridine assay

Thirty minutes before euthanasia, mice received an i.t. administration of 3 mg/kg of propidium iodide (PI) (P4170-10MG, Sigma), followed by prompt freezing of lung tissue samples in liquid nitrogen and embedding in OCT compound. The subsequent steps adhered

to established immunofluorescence protocols. For the 5-ethynyl-2'-deoxyuridine (EdU) assay, mice were i.p. injected with 100 mg/kg of EdU (ST067-50mg, Beyotime) 24 h prior to euthanasia. Following this, lung tissue samples were rapidly frozen in liquid nitrogen and embedded in OCT compound. Subsequent procedures were carried out in accordance with the prescribed protocols for immunofluorescence and utilized the BeyoClick™ EdU-488 Cell Proliferation Assay Kit (C0071S, Beyotime).

Quantitative real-time polymerase chain reaction (PCR)

Fresh lung tissues were promptly cryopreserved using liquid nitrogen to maintain tissue freshness. RNA extraction followed the TRIzol (15596018, Invitrogen) extraction protocol. The PrimeScript™ IV 1st strand complementary DNA (cDNA) Synthesis Mix (6215A, TaKaRa, Otsu, Shiga, Japan) was employed for cDNA synthesis. Subsequently, the CFX96 Real-Time System (Bio-Rad, Hercules, California, USA) in conjunction with SYBR Premix Ex Taq (RR420A, TaKaRa) was used for real-time PCR analysis. The primer sequences for *Tnf-α*, *Il-6* and *Acta2* and control *Gapdh* have been previously described.

Lung wet to dry weight ratio

Fresh lung tissues were harvested from mice and expeditiously weighed to determine their initial wet weight. These freshly obtained samples were subsequently placed in a drying oven operating within the temperature range of 60°C to 80°C. At 24 h intervals, the tissues were reweighed until a consistent weight was achieved, at which point the final weight was recorded. The moisture content of the mouse lungs was calculated by establishing the ratio of the dry weight to the wet weight. Subsequently, the experimental data underwent statistical analysis.

Statistical analyses

The data were subjected to analysis using IBM Corporation's SPSS software (version 19.0) (Armonk, NY, USA). Descriptive statistics are presented as means ± standard errors of the means (SEM). Mann-Whitney *U* test was employed to evaluate the significance of differences among samples. For quantitative image processing, GraphPad's Prism software (version 5) (San Diego, CA, USA), and Adobe Inc.'s Photoshop software (version 5.0) (San Jose, CA, USA), were employed. *P*-value <0.05 was considered statistically significant.

Results

LPS dose-dependent induction of Parkin expression correlating with lung necroptotic cell death

The lung's response to injury is intricately tied to the severity of the insult. To investigate the lung injury response, WT mice were subjected to i.t. administration of varying doses of LPS up to 15.0 mg/kg. The mice were euthanized at 24 h post LPS administration, and lung tissue samples were collected for analysis. Macroscopic evaluation revealed an increase in both the quantity and size of dark red blood spots on the lungs, particularly notable at the 10.0 mg/kg dose and above. Histological assessments of lung injury and H&E scores confirmed these findings (Fig. 1A, B). Analysis of BALF revealed a rapid surge in the total protein content and blood cells at the 10.0 mg/kg LPS dose (Fig. 1C). WB analysis further showed a subtle expression of cleaved caspase 3 at 2.5 mg/kg LPS, which rapidly increased at 5 mg/kg and but remained at sustained levels for higher doses (Supplementary Fig. 1). Notably, TNF-α expression sharply increased at the 10 mg/kg of LPS dose, accompanied by robust phosphorylation of MLKL (Supplementary Fig. 1 and Fig. 1D). Our findings indicate that as the concentration of LPS escalated, the elevation of the apoptosis marker cleaved caspase 3 plateaued, while the levels of the necroptosis marker p-MLKL increased. This suggests

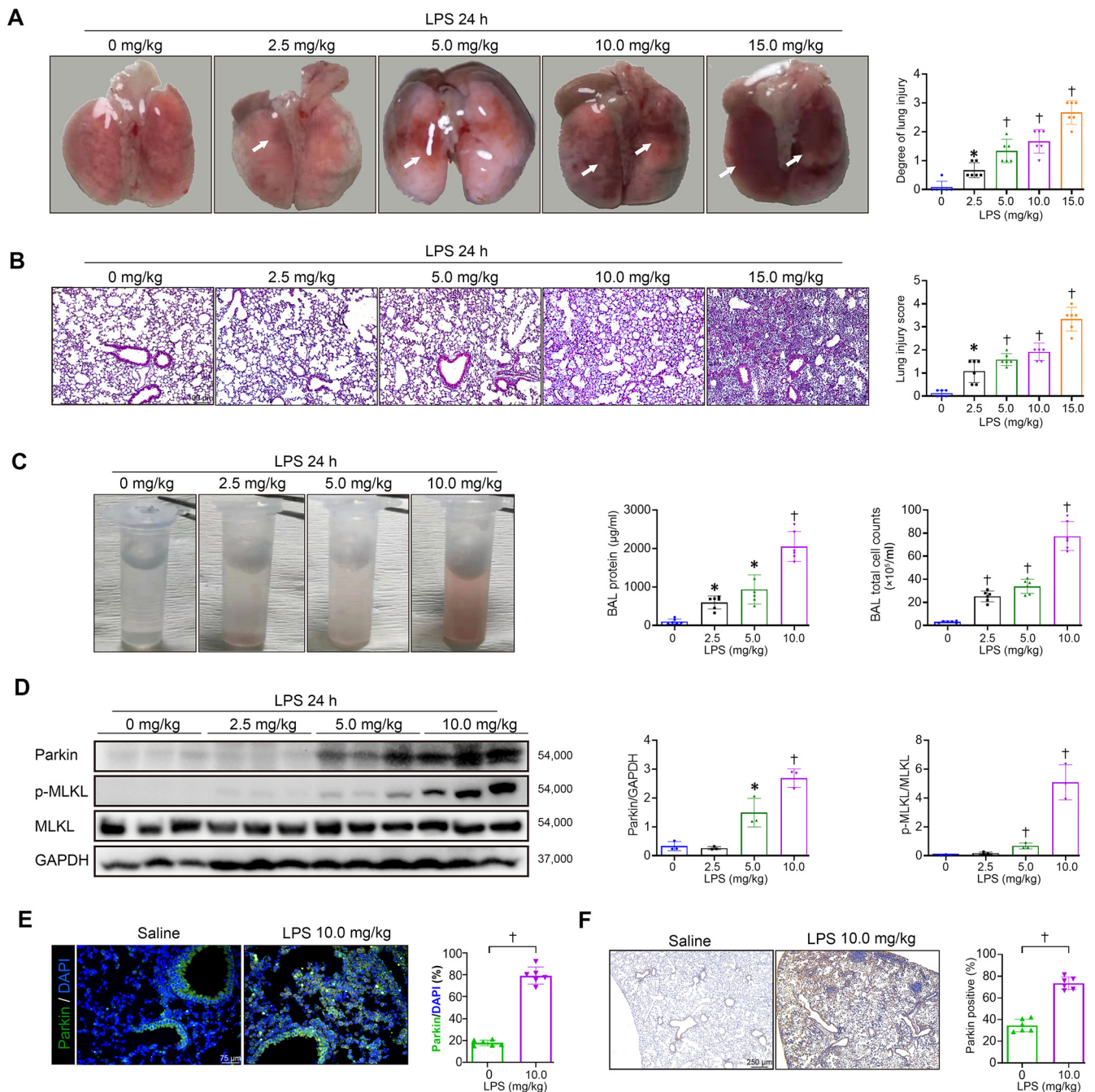


Fig. 1. LPS dose-dependent induction of Parkin expression correlates with lung necroptotic cell death. Mice were intratracheally administered varying doses of LPS as specified and sacrificed 24 h post-treatment. Lung tissues were analyzed for the following parameters: (A) Macroscopic images of mouse lungs. $n=6$. (B) Histological analysis of mouse lung tissues by H&E staining. $n=6$. (C) Visual inspection of BALF and analysis of protein and cell content in BALF. $n=6$. (D) WB analysis of Parkin and necroptosis-related marker expression in mouse lung tissues. $n=3$. (E) IF analysis of Parkin in mouse lung tissues. $n=6$. (F) IHC analysis of Parkin in mouse lung tissues. $n=6$. All data are presented as means \pm SEMs. Statistical significance is denoted as * $P < 0.05$, † $P < 0.01$ compared to LPS 0 mg/kg. Scale bar = 100 μ m for B, 75 μ m for E, 250 μ m for F. BAL: Bronchoalveolar lavage; BALF: Bronchoalveolar lavage fluid; CTRL: Control; DAPI: 4',6-diamidino-2-phenylindole; GAPDH: Glyceraldehyde-3-phosphate dehydrogenase; H&E staining: Hematoxylin and eosin staining; IF: Immunofluorescence; IHC: Immunohistochemistry; LPS: Lipopolysaccharide; MLKL: Mixed lineage kinase domain-like protein; p-MLKL: Phospho-MLKL; SEM: Standard error of the mean; WB: Western blot.

a shift in the form of lung injury from apoptosis to necroptosis under the influence of high-dose LPS. Moreover, the induction of pulmonary inflammation was strongly associated with the onset of necroptosis. Notably, Parkin expression exhibited an upsurge starting at the 5.0 mg/kg LPS dose and further increased at 10.0 mg/kg, aligning with the activation of necroptosis (Fig. 1D). The consistency of highly-induced Parkin expression was further confirmed through IF and IHC analyses (Fig. 1E and F).

MLKL depletion mitigates LPS-induced ALI

To assess the involvement of necroptosis in high-dose LPS-induced lung injury, MLKL null mice ($Mkl^{-/-}$) and WT mice ($Mkl^{+/+}$) were subjected to i.t. administration of either 10.0 mg/kg of LPS or the solvent for 24 h before being euthanized for analysis (Fig. 2A). Remarkably, $Mkl^{-/-}$ mice exhibited significantly alleviated weight loss induced by LPS compared to $Mkl^{+/+}$ mice (Fig. 2B). Histological examination using

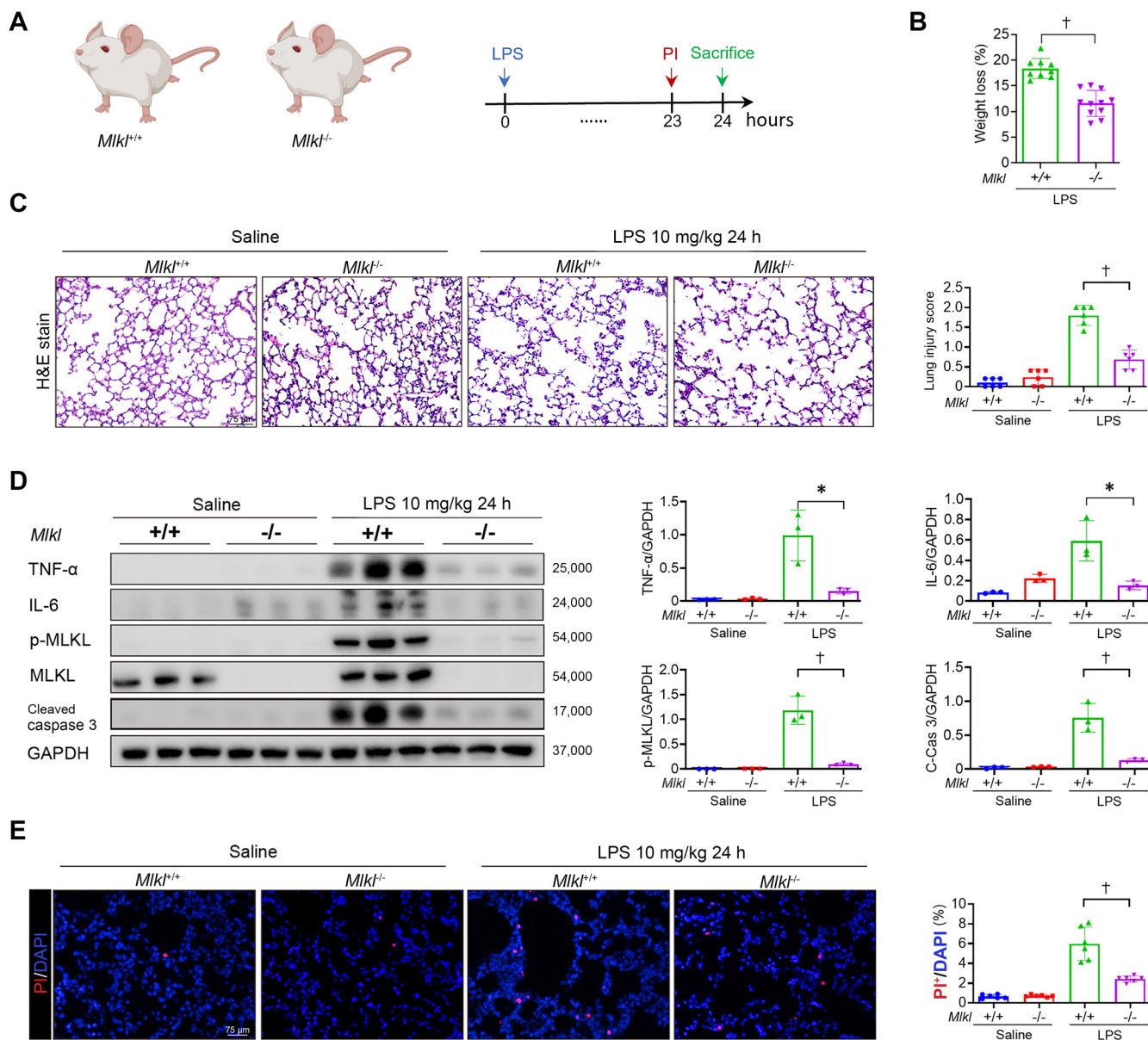


Fig. 2. MLKL depletion mitigates LPS-induced ALI. WT or MLKL null mice were sacrificed at 24 h after LPS (10.0 mg/kg) administration for the following analyses: (A) Schematic representation of the mouse model and treatment. $n=9$. (B) Graph depicting the changes in body weight in mice. (C) Histological analysis of mouse lung tissues by H&E staining. $n=6$. (D) WB analysis showing the expression of inflammatory, apoptotic, and necroptotic-related proteins in mouse lung tissues. $n=3$. (E) IF analysis of PI-stained cells in the mouse lung tissue sections. $n=6$. All data are presented as means \pm SEMs. Statistical significance is denoted as $^*P < 0.05$, $^\dagger P < 0.01$. Scale bar=75 μ m for (C) and (E). ALI: Acute lung injury; CTRL: Control; C-Cas3: Cleaved caspase 3; DAPI: 4',6-diamidino-2-phenylindole; GAPDH: Glyceraldehyde-3-phosphate dehydrogenase; H&E staining: Hematoxylin and eosin staining; IF: Immunofluorescence; IHC: Immunohistochemistry; IL-6: Interleukin-6; LPS: Lipopolysaccharide; MLKL: Mixed lineage kinase domain-like protein; PI: Propidium iodide; p-MLKL: Phospho-MLKL; SEM: Standard error of the mean; TNF- α : Tumor necrosis factor- α ; WB: Western blot; WT: Wild-type.

H&E staining depicted a substantial reduction in LPS-induced lung injury among $Mkl^{-/-}$ mice when compared to their $Mkl^{+/+}$ counterparts (Fig. 2C). Furthermore, WB analysis demonstrated a significant decrease in the LPS-triggered expression of inflammatory cytokines TNF- α and IL-6 within the lung tissues of $Mkl^{-/-}$ mice, along with diminished levels of cleaved caspase 3 compared to $Mkl^{+/+}$ mice (Fig. 2D).

For direct visualization of necroptotic cells in mouse lung tissues, we i.t. administered PI prior to euthanasia of mice to label cells with disrupted membranes, enabling their detection using IF. The outcomes revealed a reduced number of PI-positive cells in the lungs of $Mkl^{-/-}$ mice subjected to LPS treatment compared to $Mkl^{+/+}$ mice receiving the same LPS treatment (Fig. 2E). This evidence collectively highlights that MLKL depletion significantly attenuates LPS-induced

ALI, underscoring the pivotal role of necroptosis in this pathological process.

Parkin depletion exacerbates LPS-induced inflammatory cell death

Given the significant role that Parkin has been shown to play in regulating necroptosis¹⁵ and its strong association with the necroptosis phenotype (Fig. 1D-F), we wanted to further investigate the function of Parkin in LPS-induced ALI. To accomplish this, we employed *Prkn* conditional knockout mice (*UBC^{creERT2}; Prkn^{lox/fllox}*, *Prkn* conditional knockout [cKO] mice) for our LPS treatment analysis, utilizing *Prkn^{fl/fl}* mice as the control (CTRL mice). After undergoing the tamoxifen treatment regimen, Parkin cKO mice were i.t. administered 10.0 mg/kg of LPS

or the solvent for a duration of 24 h before being euthanized for detailed analysis (Fig. 3A). Strikingly, Parkin cKO mice exhibited significantly heightened weight loss induced by LPS compared to CTRL mice (Fig. 3B). Macroscopic assessment revealed larger injury areas within the lung tissues of Parkin cKO mice following LPS treatment (Fig. 3C). H&E staining also revealed a more severe LPS-induced ALI in Parkin cKO mice (Fig. 3D). Additionally, analysis of BALF indicated elevated protein content and erythrocyte levels in Parkin cKO mice (Fig. 3E). These results collectively indicate that Parkin knockout exacerbates LPS-induced lung injury.

Further investigation into the impact of Parkin deficiency on the cell death pathways unveiled notable alterations. WB analysis demonstrated that LPS treatment escalated the expression of TNF- α and IL-6, alongside increased phosphorylation levels of key kinases within the necroptotic pathway, RIPK3, and MLKL in Parkin cKO mice (Fig. 3F). Moreover, phosphorylation levels of the key kinase in pyroptosis, GSDMD, also increased following Parkin deletion and LPS treatment, while levels of cleaved caspase 3 remained relatively unchanged in Parkin cKO mice (Fig. 3G). These findings suggest that Parkin depletion skews the cell death pattern induced by LPS toward necroptosis and pyroptosis, phenomena more closely linked to inflammation.

Blocking necroptosis pathway mitigates Parkin deficiency-induced exacerbation of ALI phenotype

To elucidate the relationship between Parkin, necroptosis, and LPS-induced ALI, we utilized the RIPK3 inhibitor GSK872 to obstruct the necroptosis pathway, then assessed the effects of LPS treatment on Parkin cKO mice (Fig. 4A). Comparative analysis revealed that Parkin cKO mice experienced a more pronounced weight loss following LPS treatment compared to CTRL mice, yet this alteration was counteracted by GSK872 treatment, resulting in a mitigated weight loss in Parkin cKO mice (Fig. 4B). Notably, H&E staining analysis showed no significant changes in LPS-induced ALI between Parkin cKO mice and CTRL mice upon GSK872 treatment (Fig. 4C). Subsequent WB analyses revealed that Parkin cKO led to an upregulation of IL-6/TNF- α and increased phosphorylation of RIPK3/MLKL, which were substantially inhibited by GSK872 treatment (Fig. 4D). Further scrutiny revealed that GSK872 treatment curbed the elevation of N-GSDMD levels induced by Parkin deletion, while levels of cleaved caspase 3 remained largely unchanged (Fig. 4E). Moreover, PI-staining results indicated that GSK872 treatment hindered the necroptotic cell death in Parkin deletion mice (Fig. 4F). In conclusion, inhibition of the necroptosis pathway through GSK872 effectively alleviates the exacerbation of ALI induced by Parkin deletion.

Sftpc-lineage targeted Parkin depletion augments LPS-induced inflammation and necroptosis in AT2 cells

AT2 cells play a pivotal role in facilitating alveolar repair and regeneration after lung injury. Protecting these cells is crucial for mitigating lung injury and promoting lung repair. In our pursuit to unravel Parkin's function within AT2 cells, we used *Sftpc*-lineage Parkin knockout and tracing mice (*Sftpc*^{icre}; *Prkn*^{fllox/fllox}; *tdTomato*^{fllox/+}, AT2-Parkin cKO group) and compared them to *Sftpc*-lineage tracing mice (*Sftpc*^{icre}; *tdTomato*^{fllox/+}, CTRL group). Mice were subjected to i.t. administration of either 10.0 mg/kg LPS or the solvent for 24 h before being euthanized for analysis (Fig. 5A). Macroscopic examination revealed a larger injury area within the lung tissues of AT2-Parkin cKO mice following LPS treatment (Fig. 5B). H&E staining demonstrated a more severe LPS-induced ALI in AT2-Parkin cKO mice (Fig. 5C). IHC results indicated a significant increase in p-MLKL and CD45 positive cells in LPS-treated AT2-Parkin cKO mice (Fig. 5C). These findings were further corroborated by WB analysis, revealing notable elevations in TNF- α , p-MLKL, p-RIPK3, and cleaved caspase 3 levels in the lung tissues of LPS-treated

AT2-Parkin cKO mice (Fig. 5D). IF analysis indicated a substantial increase in the proportion of p-MLKL positive cells among tdTomato positive cells in LPS-treated AT2-Parkin cKO mice (Fig. 5E). In conclusion, the specific knockout of *Prkn* within AT2 cells resulted in heightened lung injury, early-stage lung inflammation, and the activation of the necroptosis pathway within 24 h of LPS exposure, highlighting the importance of Parkin in protecting AT2 cells in LPS-induced ALI.

AT2-specific Parkin ablation aggravates LPS-induced lung inflammatory phenotype

To assess the impact of AT2-specific Parkin cKO on the inflammatory phase of ALI, we conducted a 10.0 mg/kg LPS or the solvent treatment for 72 h to induce inflammation (Fig. 6A). Quantitative PCR analysis unveiled a significant increase in the messenger RNA (mRNA) expression levels of *Il-6* and *Tnf- α* in the lungs of LPS-treated AT2-Parkin cKO mice (Fig. 6B). Furthermore, WB analysis demonstrated elevated levels of TNF- α , p-MLKL, p-RIPK3, and cleaved caspase 3 within the lung tissues of LPS-treated AT2-Parkin cKO mice (Fig. 6C). Notably, the wet-to-dry weight ratio was found to be elevated in LPS-treated AT2-Parkin cKO mice indicating more severe pulmonary edema (Fig. 6D). Histological examinations via H&E staining revealed extensive cellular inflammatory infiltration within the alveolar region of LPS-treated AT2-Parkin cKO mice, indicating severe inflammation (Fig. 6E). IHC staining for CD45 and CD68 further substantiated that these infiltrating cells were predominantly neutrophils or macrophages, pronounced and severe inflammatory response within the lung tissues of LPS-treated AT2-Parkin cKO mice (Fig. 6E). Moreover, an increased number of HMGB1-positive cells within the alveoli of AT2-Parkin cKO mice reflected heightened release of DAMPs due to necroptotic cell membrane disruption (Fig. 6E). Therefore, AT2-Parkin cKO also led to a more pronounced lung inflammation during the inflammatory phase, highlighting the crucial role of Parkin within the broad AT2 lineage in modulating pulmonary inflammation.

Parkin deficiency in AT2 cells suppresses AT2 cell-autonomous proliferation and differentiation into AT1

AT2 cells play a critical role in lung injury repair, including proliferation and differentiation into AT1 cells. To investigate the impact of Parkin on AT2 cell proliferation and differentiation, we performed analyses on the lungs of AT2-Parkin cKO mice at day 7 post 10.0 mg/kg LPS treatment, a critical time point for AT2 cell proliferation and differentiation (Fig. 7A). The *Sftpc*^{icre}-driven tdTomato reporter showed high specificity and efficacy in marking AT2 cells (Fig. 7B). Results from SPC and EdU co-staining indicated a notable reduction in the proportion of SPC-positive cells in AT2-Parkin cKO mice, while the proportion of EdU-positive cells remained relatively unchanged (Fig. 7C). However, AT2-Parkin cKO mice exhibited a significant decrease in the proportion of SPC- and EdU- double positive cells (Fig. 7C). Based on these data, it is evident that Parkin deficiency in AT2 cells negatively impacts autonomous proliferative capacity of AT2 cells. This conclusion is further supported by *Sftpc*-lineage tracing, which revealed a noticeable decrease in the proportions of both EdU-positive and SPC-positive cell within the tdTomato-positive cells (Fig. 7D). Notably, AT2-specific Parkin deficiency also resulted in a reduced proportion of alveolar RAGE-positive AT1 cells within tdTomato-positive cells (Fig. 7D). These cumulative findings underscore the additional role of Parkin in facilitating the differentiation of AT2 into AT1, which is vital for repairing lung injury and restoring lung function.

Parkin deficiency in AT2 cells exacerbates LPS-induced pulmonary fibrosis phenotype

Amidst the progression of severe lung injury and inflammation, the emergence of pulmonary fibrosis stands as a consequential outcome.

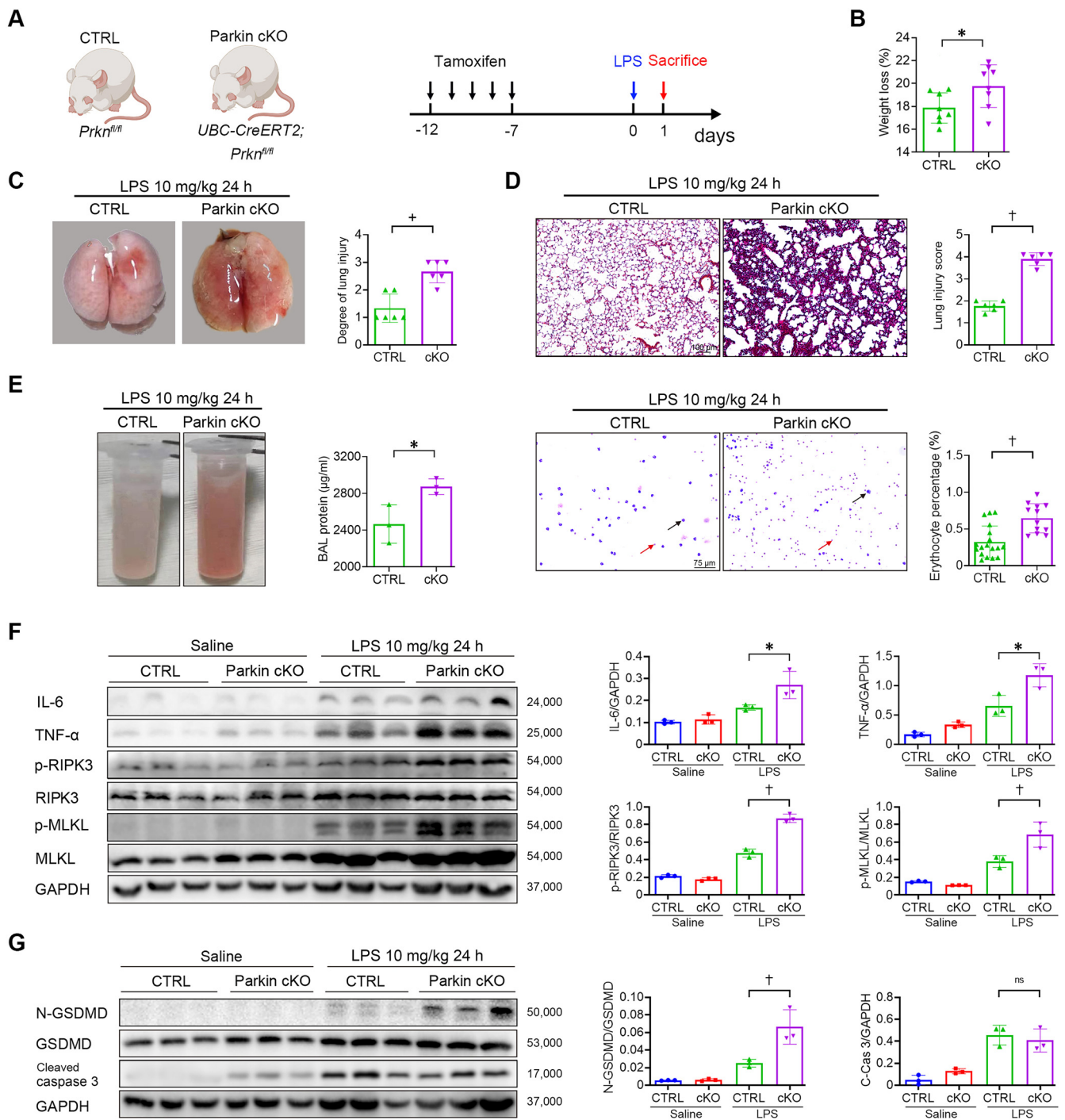


Fig. 3. Parkin depletion exacerbates LPS-induced inflammatory cell death. (A) Schematic representation of the mouse models, tamoxifen induction, and LPS (10.0 mg/kg) treatment. (B) Graph depicting the changes in body weight in mice. $n=9$. (C) Macroscopic images of mouse lungs. $n=6$. (D) Histological analysis of mouse lung tissues by H&E staining. $n=6$. (E) Analysis of BALF from mouse lung tissues (H&E staining). $n=3$. (F) WB analysis of inflammatory- and necroptosis-related proteins expression in mouse lung tissues. $n=3$. (G) Analysis of apoptotic and pyroptosis-related protein expression in mouse lung tissues. $n=3$. All data are presented as means \pm SEM. Statistical significance is denoted as * $P < 0.05$, $\dagger P < 0.01$. Scale bar = 100 μm for (D), 75 μm for (E). BAL: Bronchoalveolar lavage; BALF: Bronchoalveolar lavage fluid; C-Cas3: Cleaved caspase 3; cKO: Conditional knockout; Cre: Cyanogen bromide (CNBr)-induced recombinase; CreERT2: Cre recombinase fused to a mutated ligand-binding domain of the estrogen receptor; CTRL: Control; GAPDH: Glycerolaldehyde-3-phosphate dehydrogenase; GSDMD: Gasdermin D; H&E staining: Hematoxylin and eosin staining; IHC: Immunohistochemistry; IL-6: Interleukin-6; LPS: Lipopolysaccharide; MLKL: Mixed lineage kinase domain-like protein; p-MLKL: Phospho-MLKL; Prkn: Parkin RBR E3 ubiquitin protein ligase; p-RIPK3: Phospho-RIPK3; RIPK3: Receptor-interacting serine/threonine-protein kinase 3; SEM: Standard error of the mean; TNF- α : Tumor necrosis factor- α ; UBC: Ubiquitin C; WB: Western blot.

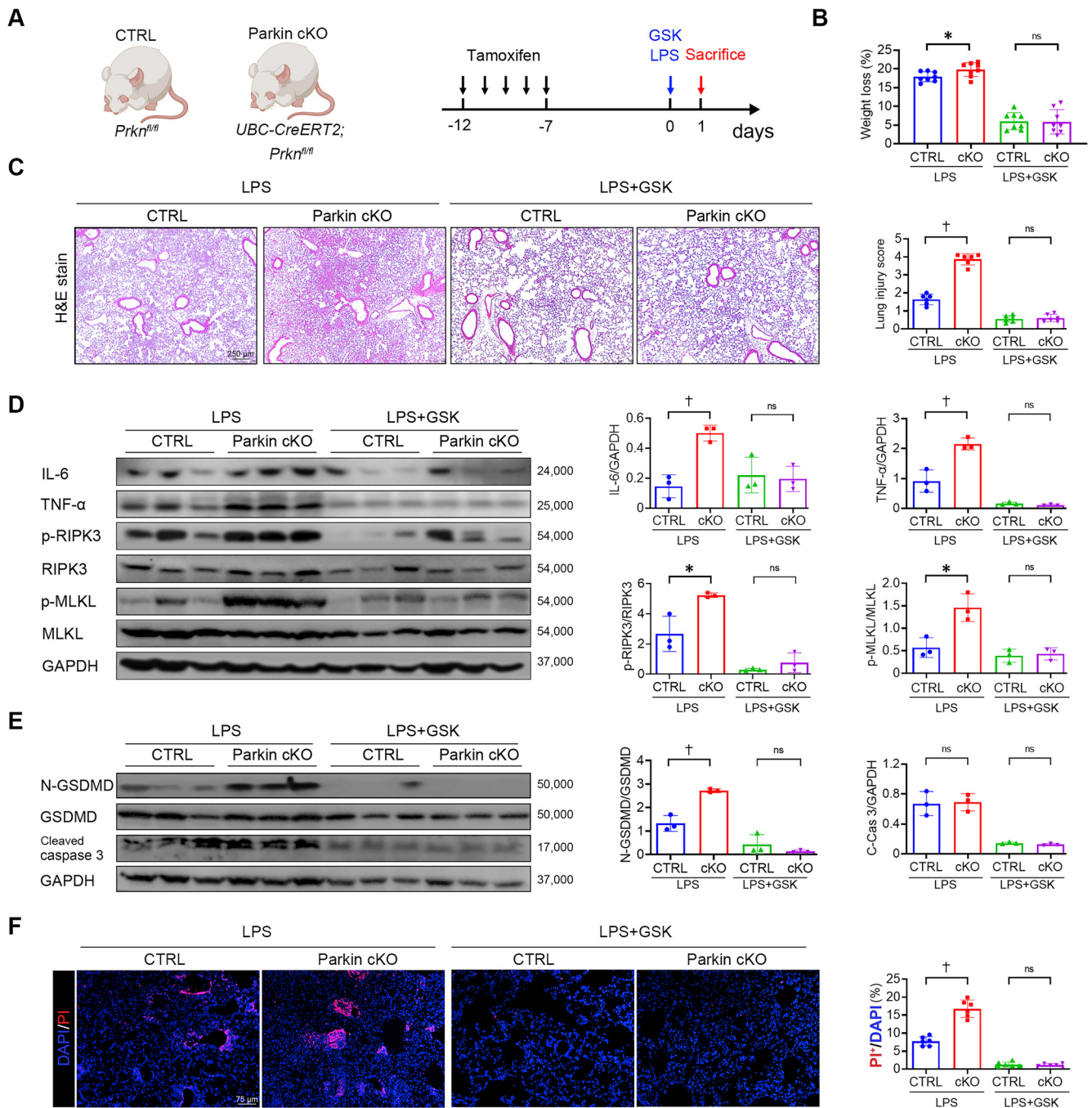


Fig. 4. Blocking necroptosis pathway mitigates Parkin deficiency-induced exacerbation of ALI phenotype. (A) Schematic representation of the mouse models, tamoxifen induction, LPS (10.0 mg/kg) and LPS/GSK872 (5.0 mg/kg) treatment regimen. (B) Graph depicting changes in body weight in mice. *n*=8. (C) Histological analysis of mouse lung tissues by H&E staining. *n*=6. (D) WB analysis of inflammatory, and necroptosis-related proteins in mouse lung tissues. *n*=3. (E) WB analysis of apoptosis- and pyroptosis-related protein expression in mouse lung tissues. *n*=3. (F) IF analysis of PI staining in the mouse lung tissues. *n*=6. All data are presented as means ± SEMs. Statistical significance is denoted as **P* < 0.05, †*P* < 0.01. Scale bar=250 μm for (C) and 75 μm for (F). ALI: Acute lung injury; C-Cas3: Cleaved caspase 3; cKO: Conditional knockout; Cre: Cyanogen bromide (CNBr)-induced recombinase; CreERT2: Cre recombinase fused to a mutated ligand-binding domain of the estrogen receptor; CTRL: Control; DAPI: 4',6-diamidino-2-phenylindole; GAPDH: Glyceraldehyde-3-phosphate dehydrogenase; GSDMD: Gasdermin D; GSK: GSK872, a highly potent, selective RIPK3 inhibitor; H&E staining: Hematoxylin and eosin staining; IF: Immunofluorescence; IHC: Immunohistochemistry; IL-6: Interleukin-6; LPS: Lipopolysaccharide; MLKL: Mixed lineage kinase domain-like protein; ns: Not significant; p-MLKL: Phospho-MLKL; PI: Propidium iodide; *Prkn*: Parkin RBR E3 ubiquitin protein ligase; p-RIPK3: Phospho-RIPK3; RIPK3: Receptor-interacting serine/threonine-protein kinase 3; SEM: Standard error of the mean; TNF-α: Tumor necrosis factor-α; UBC: Ubiquitin C; PI: Propidium Iodide; WB: Western blot.

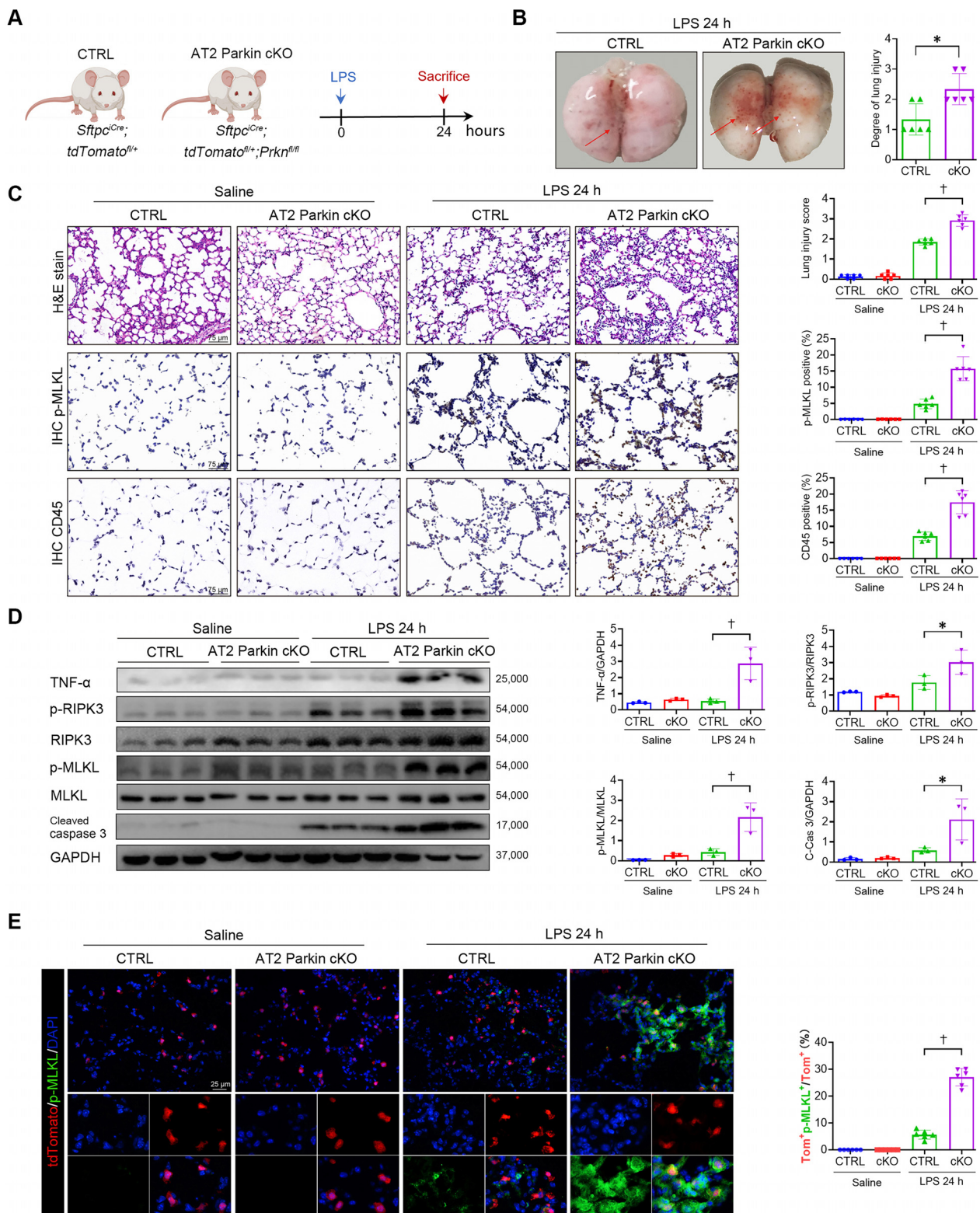


Fig. 5. *Sftpc*-lineage targeted Parkin depletion augments LPS-induced inflammation and necroptosis in AT2 cells. (A) Schematic representation of the Parkin cKO and control *Sftpc*-lineage tracing mouse models and LPS treatment regimen. (B) Macroscopic images and surface bleeding quantification. *n*=6. (C) Histological analysis by H&E staining, and IHC analysis of p-MLKL and CD45 in lung tissues. *n*=6. (D) WB analysis showing the expression of inflammation-, apoptosis-, and necroptosis-related proteins in mouse lung tissues. *n*=3. (E) IF detection and quantification of tdTomato and p-MLKL positive cells. *n*=6. All data are presented as means ± SEMs. Statistical significance is denoted as **P* < 0.05, †*P* < 0.01. Scale bar=75 μm for (C), 25 μm for (E). AT2: Alveolar type 2; C-Cas3: Cleaved caspase 3; CTRL: Control; cKO: Conditional knockout; DAPI: 4',6-diamidino-2-phenylindole; GAPDH: Glyceraldehyde-3-phosphate dehydrogenase; H&E staining: Hematoxylin and eosin staining; IF: Immunofluorescence; IHC: Immunohistochemistry; LPS: Lipopolysaccharide; MLKL: Mixed lineage kinase domain-like protein; p-MLKL: Phospho-MLKL; p-RIPK3: Phospho-RIPK3; *Prkn*: Parkin RBR E3 ubiquitin protein ligase; RIPK3: Receptor-interacting serine/threonine-protein kinase 3; SEM: Standard error of the mean; *Sftpc*: Surfactant protein C; TNF-α: Tumor necrosis factor-α; Tom: tdTomato; WB: Western blot.

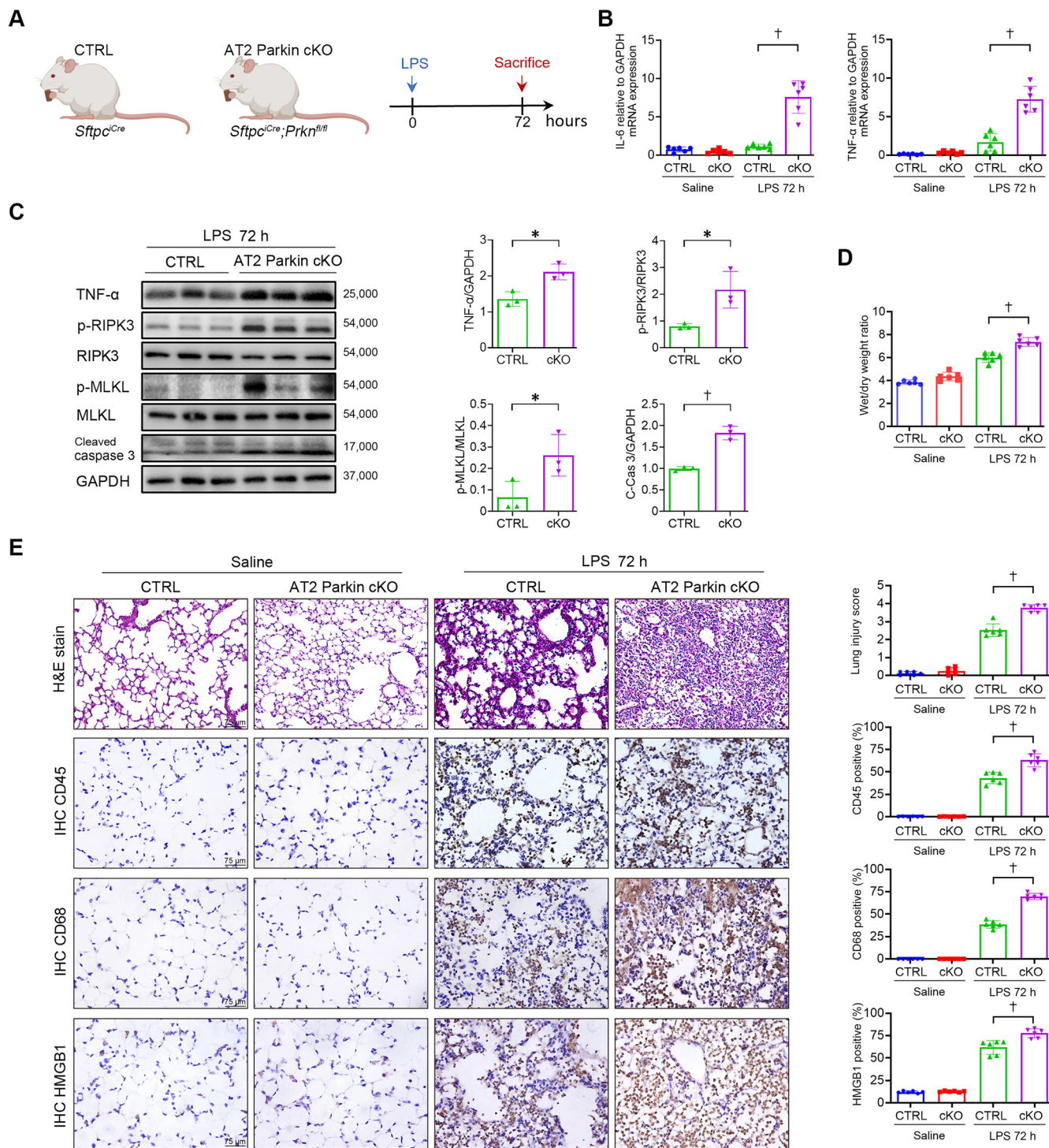


Fig. 6. AT2-specific Parkin ablation aggravates LPS-induced lung inflammatory phenotype. (A) Schematic representation of the mouse model and LPS treatment. (B) Quantitative RT-PCR analysis of *Il-6* and *Tnf- α* mRNA expression levels in lung tissues. *n*=6. (C) WB analysis showing the expression of inflammation, apoptosis, and necroptosis-related proteins in lung tissue. *n*=3. (D) Wet-to-dry weight ratio of lung tissues. *n*=6. (E) Histological analysis by H&E staining. IHC analysis of CD45, CD68 and HMGB1 in lung tissue. *n*=6. All data are presented as means \pm SEMs. Statistical significance is denoted as **P* < 0.05, †*P* < 0.01. Scale bar=75 μ m for (E). AT2: Alveolar type 2; C-Cas3: Cleaved caspase 3; CTRL: Control; cKO: Conditional knockout; GAPDH: Glyceraldehyde-3-phosphate dehydrogenase; H&E staining: Hematoxylin and eosin staining; HMGB1: High mobility group box 1; IF: Immunofluorescence; IHC: Immunohistochemistry; IL-6: Interleukin-6; LPS: Lipopolysaccharide; MLKL: Mixed lineage kinase domain-like protein; mRNA: Messenger RNA; p-MLKL: Phospho-MLKL; p-RIPK3: Phospho-RIPK3; *Prkn*: Parkin RBR E3 ubiquitin protein ligase; RIPK3: Receptor-interacting serine/threonine-protein kinase 3; RT-PCR: Reverse transcription polymerase chain reaction; SEM: Standard error of the mean; *Sftpc*: Surfactant protein C; TNF- α : Tumor necrosis factor- α ; WB: Western blot.

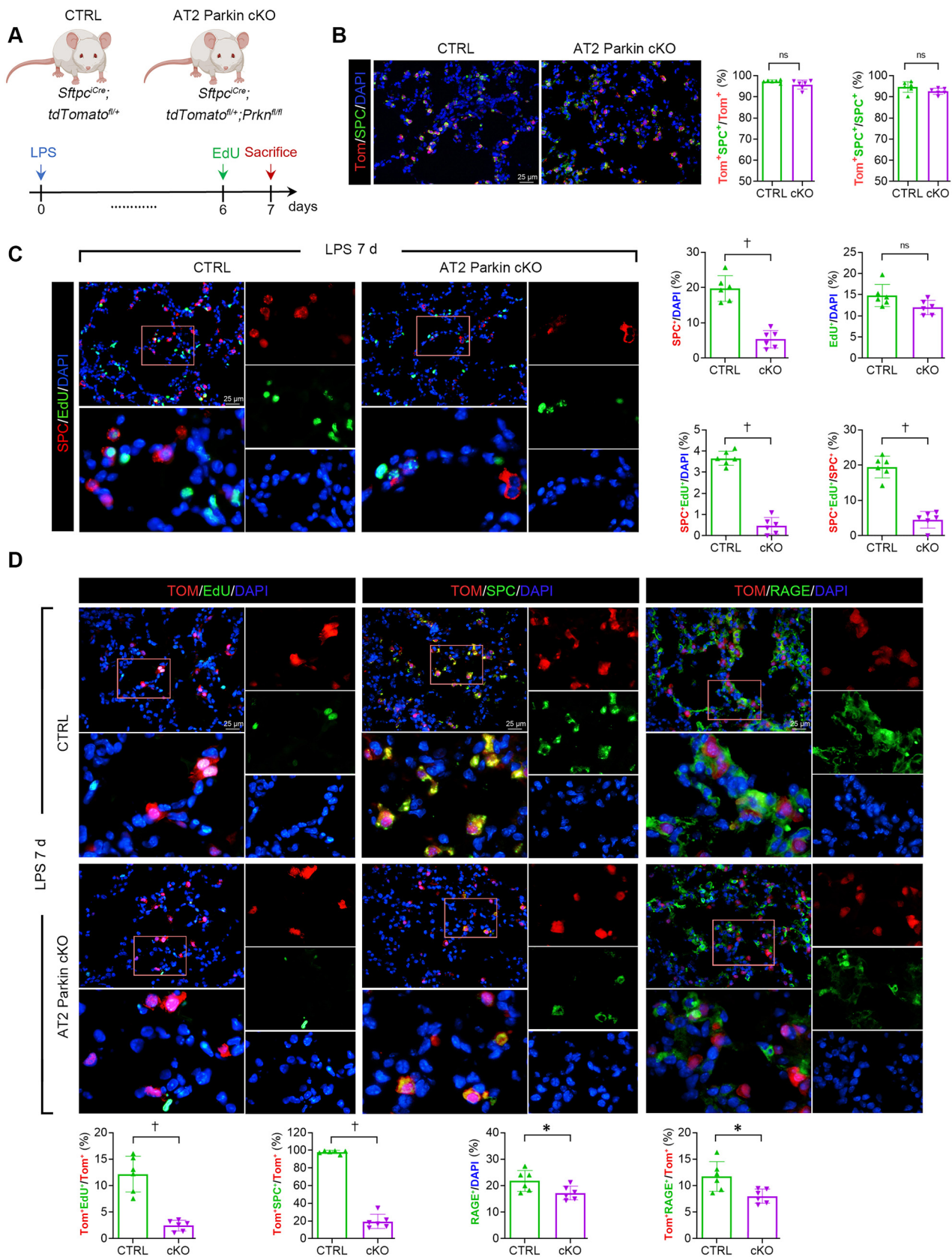


Fig. 7. Parkin deficiency in AT2 cells suppresses AT2 cell-autonomous proliferation and differentiation into AT1. (A) Schematic representation of the mouse model and treatment. (B) IF detection and quantification of tdTomato and Sftpc positive cells. *n* = 6. (C) IF detection and quantification of Sftpc and EdU positive cells. *n* = 6. (D) IF detection and quantification of tdTomato, Sftpc, EdU and RAGE positive cells. *n* = 6. All data are presented as means ± SEMs. Statistical significance is denoted as **P* < 0.05, †*P* < 0.01. Scale bar = 25 μm for (B), (C), (D). AT1: Alveolar type 1; AT2: Alveolar type 2; CTRL: Control; cKO: Conditional knockout; DAPI: 4',6-diamidino-2-phenylindole; EdU: 5-ethynyl-2'-deoxyuridine; IF: Immunofluorescence; LPS: Lipopolysaccharide; ns: Not significant; *Prkn*: Parkin RBR E3 ubiquitin protein ligase; RAGE: Receptor for advanced glycation end products; SEM: Standard error of the mean; *Sftpc*: Surfactant protein C; SPC: Surfactant protein C; Tom: tdTomato.

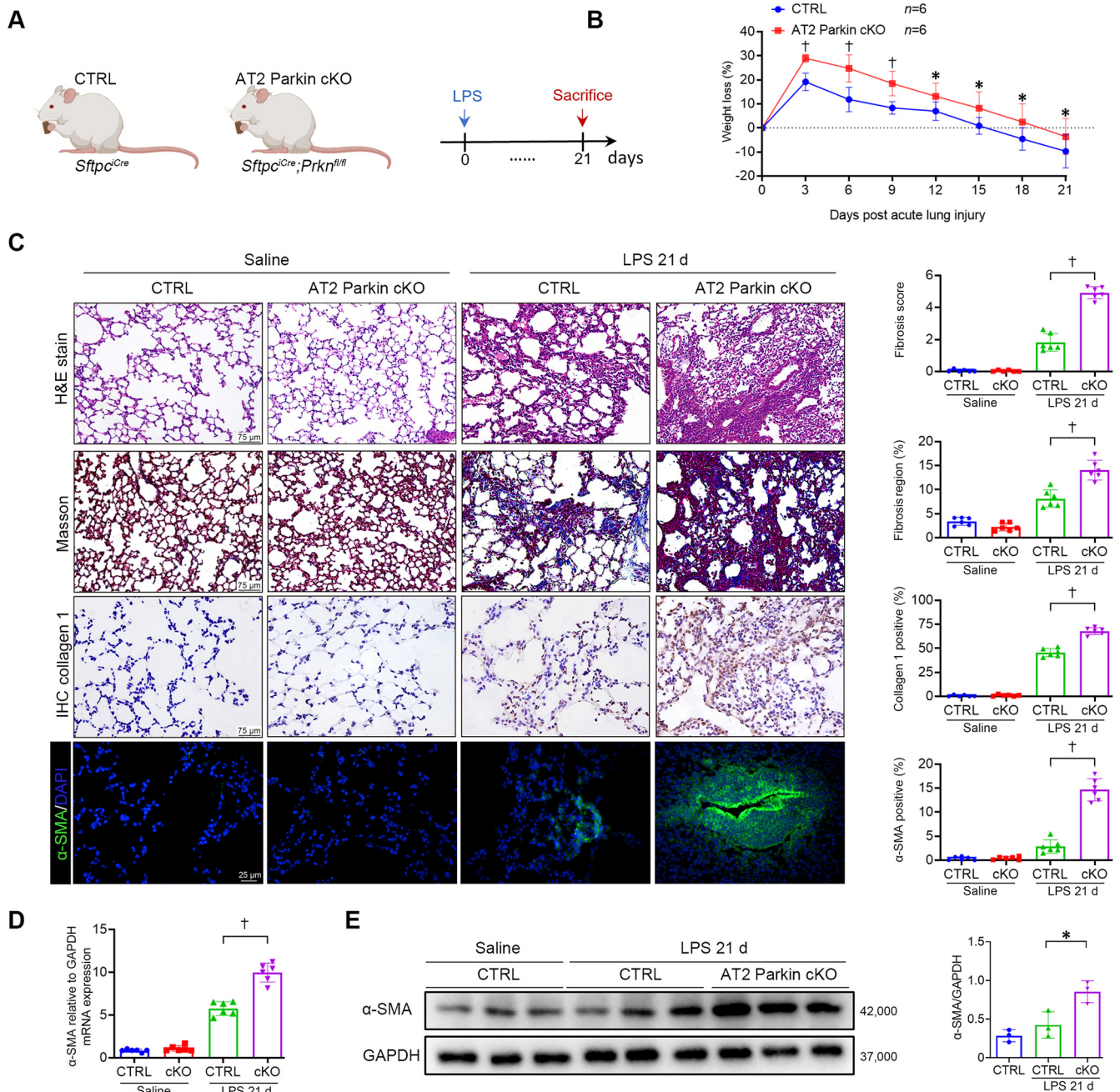


Fig. 8. Parkin deficiency in AT2 cells exacerbates LPS-induced pulmonary fibrosis. (A) Schematic representation of the mouse model and treatment. (B) Graph depicting changes in body weight in mice. $n=6$. (C) H&E staining was performed to assess lung histology and fibrosis score. Masson staining was used to detect lung tissues fibrosis. IHC and IF staining were carried out to detect Collagen 1 and α -SMA, respectively. $n=6$. (D) Quantitative RT-PCR analysis of *Acta2* (α -SMA) mRNA expression levels in lung tissues. $n=6$. (E) WB analysis showing the expression of α -SMA and quantification normalized to GAPDH. $n=3$. All data are presented as means \pm SEMs. Statistical significance is denoted as * $P < 0.05$, † $P < 0.01$. Scale bar=75 μ m or 25 μ m for (C). α -SMA: α -smooth muscle actin; AT2: Alveolar type 2; CTRL: Control; cKO: Conditional knockout; DAPI: 4',6-diamidino-2-phenylindole; GAPDH: Glyceraldehyde-3-phosphate dehydrogenase; H&E staining: Hematoxylin and eosin staining; IF: Immunofluorescence; IHC: Immunohistochemistry; LPS: Lipopolysaccharide; *Prkn*: Parkin RBR E3 ubiquitin protein ligase; RT-PCR: Reverse transcription polymerase chain reaction; SEM: Standard error of the mean; *Sftpc*: Surfactant protein C; WB: Western blot.

Therefore, we further determined the influence of AT2 cell-specific Parkin deletion on pulmonary fibrosis. Indicated mice were subjected to i.t. administration of either 10.0 mg/kg LPS or the solvent for 21 days before being euthanized for analysis (Fig. 8A). Remarkably, AT2-Parkin cKO mice exhibited significantly heightened weight loss induced by LPS compared to control mice (Fig. 8B). H&E staining revealed an intensified presence of fibroblasts within the lungs of LPS-treated AT2-Parkin cKO mice, indicating increased fibrotic activity (Fig. 8C). Sub-

sequent validation through Masson staining affirmed an augmented deposition of collagen within the lungs of LPS-treated AT2 Parkin cKO mice (Fig. 8C). IHC and IF analyses on Collagen 1 and α -SMA positive cells denoted enhanced fibrotic remodeling within the lung tissues of LPS-treated AT2-Parkin cKO mice (Fig. 8C). Consistent with these findings, both mRNA and protein analyses revealed an upregulation in α -SMA expression within the lung tissues of LPS-treated AT2-Parkin cKO mice (Fig. 8D and E). Therefore, AT2-specific Parkin deletion exacer-

bates the development of pulmonary fibrosis during the fibrotic stage of lung injury. The increased presence of fibroblasts, collagen deposition, and α -SMA expression observed in LPS-treated AT2-Parkin cKO mice indicates enhanced fibrotic remodeling and highlights the role of Parkin in mitigating fibrotic progression in lung injury.

Discussion

Unlike apoptosis, necroptosis culminates in cell membrane rupture, leading to the release of abundant cellular contents, such as DAMPs, into the extracellular matrix.²⁰ This phenomenon triggers a robust inflammatory response, fostering a feedback loop between cellular injury and inflammation, thereby exacerbating tissue damage. Hence, restraining necroptosis assumes greater significance in safeguarding the lung from severe damage. Numerous studies corroborate the notion that curbing necroptosis reduces tissue damage prompted by inflammation.²¹ However, conflicting reports exist, suggesting that in specific inflammatory damage models, inhibiting necroptosis did not confer protective effects.²² We postulate that the intensity of the injury might account for this discrepancy. Our observations revealed that under a 5 mg/kg LPS treatment, MLKL activation was not notably significant, while caspase 3 displayed substantial activation (Supplementary Fig. 1). This implies that under low-dose damage conditions, inhibiting necroptosis may not offer protection. Conversely, elevating the LPS dose from 5.0 mg/kg to 10.0 mg/kg did not significantly alter Caspase-3 activity, yet substantially activated MLKL. This suggests that activation of necroptosis pathway contributes to degree of mouse lung injury at the 10.0 mg/kg dose, the dosage chosen for our experiment. In summary, there was a significant reduction in lung injury induced by high-dose LPS in mice through necroptosis inhibition. The findings together suggest that the protective efficacy of necroptosis inhibition may be influenced by the extent of tissue damage. The intricate interplay between the severity of injury and the effectiveness of necroptosis inhibition warrants further investigation to elucidate the underlying mechanisms and potential therapeutic implications.

Parkin, an E3 ligase, orchestrates substrate ubiquitination, modulating their stability and fate, as well as their functional dynamics. Historically, investigations into Parkin predominantly focused on its impact within mitochondria. Parkin's role in fostering impaired mitophagy by ubiquitinating PINK1 has been extensively documented, thereby impeding injury-induced apoptosis.²³ Our previous study unveils a novel facet of Parkin's functionality: it hampers RIPK3 phosphorylation by ubiquitinating RIPK3, consequently thwarting necroptosis via the Parkin–RIPK3–MLKL axis.¹⁵ In this study, we observed that Parkin expression was upregulated in response to 5 mg/kg and 10 mg/kg LPS treatment (Figure 1D–F). This suggests that Parkin is an injury-activated protein that may play a role in the repair of pulmonary damage. Our results reveal that either *Ubc*-driven systemic (Fig. 3) or *Sftpc*-lineage *Prkn* knock-out (Fig. 5) in adult mice exacerbates high dose LPS-induced epithelial necroptosis and ALI phenotype. Significantly, inhibition of necroptosis partially reversed the exacerbated damaging phenotype resulting from Parkin deletion (Fig. 4). Although the results underscore a pivotal role of the Parkin–RIPK3–MLKL axis in ALI, our observations do not preclude Parkin's potential role in ALI via regulating other death pathways such as apoptosis and/or pyroptosis. Notably, literature suggests the potential interconversion of necroptosis and apoptosis under specific conditions.²⁴ Indeed, our data revealed that, in systemic Parkin cKO mice subjected to LPS induction, there was no significant increase in cleaved Caspase-3 levels (Fig. 4E). In contrast, AT2-specific Parkin cKO mice exhibited a significant elevation in cleaved-Caspase3 levels (Figs. 5D and 6C). One plausible explanation is that systemic Parkin cKO precipitates severe lung injury, favoring a predominant pattern of necroptotic cell death in lung cells. Conversely, AT2-specific Parkin cKO, inducing comparatively lesser damage to lung tissues, instigates a simultaneous occurrence of apoptosis and necroptosis. Another conjecture is that AT2-specific Parkin cKO instigates extensive necroptosis among AT2 cells,

exacerbating lung inflammation and triggering apoptosis in non-AT2 lung cells. It's important to note that these scenarios may coexist and necessitate further probing to unravel their interplay.

Parkin activity can be stimulated via AMPK activation.¹⁵ The AMPK pathway plays a pivotal role in monitoring the energy status of eukaryotic cells, triggered by a decline in intracellular ATP levels and an elevation in the AMP/ATP ratio.²⁵ Metformin (Glucophage), a well-known AMPK agonist, has garnered extensive recognition among patients with diabetes, obesity, and cardiovascular diseases, with its established safety profile.²⁶ Recent findings have demonstrated metformin's efficacy in ameliorating various injuries in animal models, including lung injury and fibrosis.^{27,28} Our previous study showcased metformin's capacity to expedite fibrosis regression by prompting the myofibroblast to lipofibroblast transition.²⁹ Our recent study has reported that metformin inhibits necroptosis and mitigates B[a]P-induced chronic lung inflammation and pulmonary fibrosis.²⁹ In addition to metformin, a number of other drugs and natural compounds exhibiting anti-inflammatory or tissue-protective properties have been identified as AMPK activators, such as Berberine,³⁰ Resveratrol,³¹ Curcumin,³² and Epigallocatechin gallate (EGCG).³³ These investigations have corroborated the use of AMPK agonists for their anti-inflammatory and tissue-protective effects. The involvement of the Parkin–RIPK3–MLKL axis may potentially underlie the effectiveness of AMPK agonists. Overall, Parkin stands as a valuable clinical target in combatting inflammation and injury.

In addition to their role in surfactant production, regulation of alveolar fluid dynamics, and innate immune responses, AT2 cells stand as pivotal sources of facultative stem cells crucial for epithelial repair and regeneration.³⁴ The absence of AT2 cells within the human lung structure leads to irreversible pulmonary fibrosis.³⁵ Consequently, safeguarding the integrity of AT2 cells holds paramount significance in mitigating lung injury and facilitating lung tissues repair. Our findings illustrate that the targeted knockdown of Parkin within *Sftpc*-lineage cells exacerbated LPS-induced necroptosis in AT2 cells (Fig. 5), lung inflammation (Fig. 6), and subsequent lung fibrosis phenotype (Fig. 8). Thus, these data strongly support the assertion that Parkin's protective effect against lung injury predominantly emanates from its role in preserving AT2 cells and their stem cell activity.

Besides its impact on epithelial necroptosis, additional roles of Parkin on AT2 cell proliferation and AT2-to-AT1 differentiation are also implicated. Notably, a significant reduction in RAGE and tdTomato double positive cells in AT2-Parkin cKO mice were observed (Fig. 7D). However, such alteration was not as pronounced as the change in the number and percentage of tdTomato and EdU positive cells. Hence, the likelihood persists that Parkin fosters AT2 cell survival, consequently indirectly preserving the regenerative capacity of AT2 cells to differentiate into AT1 cells. However, our results do not exclude the possibility that Parkin directly influences the differentiation of AT2 cells into AT1 cells. Parkin is recognized as an important protein in the regulation of mitochondrial function and cellular energy metabolism.³⁶ The differentiation of AT2 cells into AT1 cells is an energetically demanding process. Recent literature has reported that AMPK-6-phosphofructo-2-kinase/fructose-2,6-biphosphatase 2 (PFKFB2) signaling upregulates glycolysis, which is essential for supporting the intracellular energy expenditure required for cytoskeletal remodeling during AT2 cell differentiation.³⁷ However, there is no evidence indicating Parkin's involvement in this process.

In summary, this study reveals the protective role of the Parkin–RIPK3–MLKL axis in suppressing necroptosis within AT2 cells and mitigating high-dose LPS induced injury. These findings support the potential activation of Parkin as a viable strategy to alleviate inflammation-triggered ALI and its associated complications. Moreover, targeting Parkin demonstrates therapeutic potential in preserving AT2 cells and their regenerative capacity. This multifaceted role of Parkin in ALI suggests its promise as a potential clinical target for combating inflammation and injury, warranting further investigation into underlying mechanisms and therapeutic implications. Future research should focus on

understanding the molecular mechanisms and the potential translation of targeting Parkin in the context of ALI therapy.

Declaration of competing interest

The authors have no relevant financial or non-financial interests to disclose.

Funding

The study was partially supported by the [National Natural Science Foundation of China](#) (Nos. 82370085 and 82170017 to CC). JSZ received partial funding from the [Zhejiang Province Public Welfare Fund Project](#) (No. LY24H050003), the [Discipline Cluster of Oncology at Wenzhou Medical University](#), China (No. Z1-2023004), as well as startup research funds from both the [Quzhou Affiliated Hospital](#) and [The First Affiliated Hospital of Wenzhou Medical University](#).

Supplementary materials

Supplementary material associated with this article can be found, in the online version, at [doi:10.1016/j.pccm.2024.11.004](https://doi.org/10.1016/j.pccm.2024.11.004).

References

- Bellani G, Laffey JG, Pham T, et al. Epidemiology, patterns of care, and mortality for patients with acute respiratory distress syndrome in intensive care units in 50 countries. *JAMA*. 2016;315:788–800. doi:10.1001/jama.2016.0291.
- Marchionni A, Tonelli R, Ball L, et al. Acute exacerbation of idiopathic pulmonary fibrosis: lessons learned from acute respiratory distress syndrome. *Crit Care*. 2018;22:80. doi:10.1186/s13054-018-2002-4.
- Matthay MA, Zemans RL, Zimmerman GA, et al. Acute respiratory distress syndrome. *Nat Rev Dis Primers*. 2019;5:18. doi:10.1038/s41572-019-0069-0.
- Wu H, Tang N. Stem cells in pulmonary alveolar regeneration. *Development*. 2021;148:dev193458. doi:10.1242/dev.193458.
- Zhang J, Liu Y. Epithelial stem cells and niches in lung alveolar regeneration and diseases. *Chin Med J Pulm Crit Care Med*. 2024;2:17–26. doi:10.1016/j.pccm.2023.10.007.
- Chong L, Ahmadvand N, Noori A, et al. Injury activated alveolar progenitors (IAAPs): the underdog of lung repair. *Cell Mol Life Sci*. 2023;80:145. doi:10.1007/s00018-023-04789-6.
- Alvarez-Palomo B, Sanchez-Lopez LI, Moodley Y, Edel MJ, Serrano-Mollar A. Induced pluripotent stem cell-derived lung alveolar epithelial type II cells reduce damage in bleomycin-induced lung fibrosis. *Stem Cell Res Ther*. 2020;11:213. doi:10.1186/s13287-020-01726-3.
- Roverato ND, Sailer C, Catone N, Aichem A, Stengel F, Groettrup M. Parkin is an E3 ligase for the ubiquitin-like modifier FAT10, which inhibits Parkin activation and mitophagy. *Cell Rep*. 2021;34:108857. doi:10.1016/j.celrep.2021.108857.
- Quinn P, Moreira PI, Ambrósio AF, Alves CH. PINK1/PARKIN signalling in neurodegeneration and neuroinflammation. *Acta Neuropathol Commun*. 2020;8:189. doi:10.1186/s40478-020-01062-w.
- Baaske MK, Kramer ER, Meka DP, Engler G, Engel AK, Moll C. Parkin deficiency perturbs striatal circuit dynamics. *Neurobiol Dis*. 2020;137:104737. doi:10.1016/j.nbd.2020.104737.
- Kitada T, Asakawa S, Hattori N, et al. Mutations in the parkin gene cause autosomal recessive juvenile parkinsonism. *Nature*. 1998;392:605–608. doi:10.1038/33416.
- Zhang Z, Chen Z, Liu R, et al. Bcl-2 proteins regulate mitophagy in lipopolysaccharide-induced acute lung injury via PINK1/parkin signaling pathway. *Oxid Med Cell Longev*. 2020;2020:6579696. doi:10.1155/2020/6579696.
- Letsiou E, Sammani S, Wang H, Belvitch P, Dudek SM. Parkin regulates lipopolysaccharide-induced proinflammatory responses in acute lung injury. *Transl Res*. 2017;181:71–82. doi:10.1016/j.trsl.2016.09.002.
- Lee S, She J, Deng B, et al. Multiple-level validation identifies PARK2 in the development of lung cancer and chronic obstructive pulmonary disease. *Oncotarget*. 2016;7:44211–44223. doi:10.18632/oncotarget.9954.
- Lee SB, Kim JJ, Han SA, et al. The AMPK-Parkin axis negatively regulates necroptosis and tumorigenesis by inhibiting the necrosome. *Nat Cell Biol*. 2019;21:940–951. doi:10.1038/s41556-019-0356-8.
- Royce GH, Brown-Borg HM, Deepa SS. The potential role of necroptosis in inflammation and aging. *Geroscience*. 2019;41:795–811. doi:10.1007/s11357-019-00131-w.
- Liu M, Li H, Yang R, Ji D, Xia X. GSK872 and necrostatin-1 protect retinal ganglion cells against necroptosis through inhibition of RIP1/RIP3/MLKL pathway in glutamate-induced retinal excitotoxic model of glaucoma. *J Neuroinflammation*. 2022;19:262. doi:10.1186/s12974-022-02626-4.
- Rodríguez DA, Weinlich R, Brown S, et al. Characterization of RIPK3-mediated phosphorylation of the activation loop of MLKL during necroptosis. *Cell Death Differ*. 2016;23:76–88. doi:10.1038/cdd.2015.70.
- Quan MY, Yan X, Miao W, et al. Metformin alleviates benzo[a]pyrene-induced alveolar injury by inhibiting necroptosis and protecting AT2 cells. *Ecotoxicol Environ Saf*. 2024;272:116094. doi:10.1016/j.ecoenv.2024.116094.
- Chen R, Kang R, Tang D. The mechanism of HMGB1 secretion and release. *Exp Mol Med*. 2022;54:91–102. doi:10.1038/s12276-022-00736-w.
- Avishekh G, David F B, Sameer N, et al. Necroptosis blockade prevents lung injury in severe influenza. *Nature*. 2024;628:835–843. doi:10.1038/s41586-024-07265-8.
- Fritsch M, Günther SD, Schwarzer R, et al. Caspase-8 is the molecular switch for apoptosis, necroptosis and pyroptosis. *Nature*. 2019;575:683–687. doi:10.1038/s41586-019-1770-6.
- Li W, Jiang WS, Su YR, et al. PINK1/Parkin-mediated mitophagy inhibits osteoblast apoptosis induced by advanced oxidation protein products. *Cell Death Dis*. 2023;14:88. doi:10.1038/s41419-023-05595-5.
- Bertheloot D, Latz E, Franklin BS. Necroptosis, pyroptosis and apoptosis: an intricate game of cell death. *Cell Mol Immunol*. 2021;18:1106–1121. doi:10.1038/s41423-020-00630-3.
- Garcia D, Shaw RJ. AMPK: mechanisms of cellular energy sensing and restoration of metabolic balance. *Mol Cell*. 2017;66:789–800. doi:10.1016/j.molcel.2017.05.032.
- Luo F, Das A, Chen J, Wu P, Li X, Fang Z. Metformin in patients with and without diabetes: a paradigm shift in cardiovascular disease management. *Cardiovasc Diabetol*. 2019;18:54. doi:10.1186/s12933-019-0860-y.
- Rangarajan S, Bone NB, Zmijewska AA, et al. Metformin reverses established lung fibrosis in a bleomycin model. *Nat Med*. 2018;24:1121–1127. doi:10.1038/s41591-018-0087-6.
- Wu L, Cen Y, Feng M, et al. Metformin activates the protective effects of the AMPK pathway in acute lung injury caused by paraquat poisoning. *Oxid Med Cell Longev*. 2019;2019:1709718. doi:10.1155/2019/1709718.
- Kheirollahi V, Wasnick RM, Biasin V, et al. Metformin induces lipogenic differentiation in myofibroblasts to reverse lung fibrosis. *Nat Commun*. 2019;10:2987. doi:10.1038/s41467-019-10839-0.
- Zhu X, Bian H, Wang L, et al. Berberine attenuates nonalcoholic hepatic steatosis through the AMPK-SREBP-1c-SCD1 pathway. *Free Radic Biol Med*. 2019;141:192–204. doi:10.1016/j.freeradbiomed.2019.06.019.
- Huang Y, Zhu X, Chen K, et al. Resveratrol prevents sarcopenic obesity by reversing mitochondrial dysfunction and oxidative stress via the PKA/LKB1/AMPK pathway. *Aging (Albany NY)*. 2019;11:2217–2240. doi:10.18632/aging.101910.
- Jin Z, Chang B, Wei Y, et al. Curcumin exerts chondroprotective effects against osteoarthritis by promoting AMPK/PINK1/Parkin-mediated mitophagy. *Biomed Pharmacother*. 2022;151:113092. doi:10.1016/j.biopha.2022.113092.
- Zhou Y, Huang S, Guo Y, et al. Epigallocatechin gallate circumvents drug-induced resistance in non-small-cell lung cancer by modulating glucose metabolism and AMPK/AKT/MAPK axis. *Phytother Res*. 2023;37:5837–5853. doi:10.1002/ptr.7990.
- Nabhan AN, Brownfield DG, Harbury PB, Krasnow MA, Desai TJ. Single-cell Wnt signaling niches maintain stemness of alveolar type 2 cells. *Science*. 2018;359:1118–1123. doi:10.1126/science.aam6603.
- Yao C, Guan X, Carraro G, et al. Senescence of alveolar type 2 cells drives progressive pulmonary fibrosis. *Am J Respir Crit Care Med*. 2021;203:707–717. doi:10.1164/rccm.202004-1274OC.
- Li J, Yang D, Li Z, et al. PINK1/Parkin-mediated mitophagy in neurodegenerative diseases. *Ageing Res Rev*. 2023;84:101817. doi:10.1016/j.arr.2022.101817.
- Wang Z, Wei D, Bin E, et al. Enhanced glycolysis-mediated energy production in alveolar stem cells is required for alveolar regeneration. *Cell Stem Cell*. 2023;30:1028–1042.e7. doi:10.1016/j.stem.2023.07.007.